Bifurcations of closed orbits in singlet helium Stark spectra

Annemieke Kips, Wim Vassen, and Wim Hogervorst
Department of Physics and Astronomy, Vrije Universiteit, De Boelelaan 1081, 1081 HV Amsterdam, The Netherlands
(Received 25 September 1998)

We measured constant-scaled-energy $M=0$ spectra of helium Rydberg atoms ($n=55$ to 80) in an electric field, allowing for a test of closed-orbit theory under conditions where bifurcations from the uphill and downhill orbits are important. Recent advances in the theory (uniform approximation) were implemented for a comparison with experimental data. The observed recurrence spectra could be explained in detail as far as the actions of all hydrogenic orbits and the intensities of most recurrences are concerned. Additional peaks in the recurrence spectra that correspond to orbits with an action equal to the sum of two hydrogenic orbits were attributed to scattering at the He^+ core. This was confirmed in a closed-orbit calculation including the quantum defects in helium. Small changes in the recurrence strength of the hydrogenic orbits were found both in experimental recurrence spectra and in the closed-orbit calculation for helium, and could be ascribed to the effect of core shadowing. [S1050-2947(99)07104-8]

PACS number(s): 32.60.+i, 32.80.Rm, 03.65.Sq

I. INTRODUCTION

The semiclassical closed-orbit theory [1–4] has been developed to explain the oscillations in the absorption spectrum of a highly excited hydrogen atom in an external field. A closed classical electron orbit that starts from the nucleus and, after traveling in the combined Coulomb-external-field potential, returns to the nucleus contributes a deformed sine oscillation to the absorption spectrum. Its frequency relates to the classical action along the orbit and its amplitude to the stability of the orbit, the ground state from which the excitation is started, and the polarization of the laser with respect to the applied field.

The closed orbits of a system are most accurately studied under constant classical conditions. For this purpose a scaling property of the classical Hamiltonian of the hydrogen atom in an electric field can be exploited. The scaled Hamiltonian does not depend on electric field F and energy E separately, but solely on the scaled energy $\epsilon = E/\sqrt{F}$ (energy E and electric field F both in atomic units). The classical dynamics are completely determined by this scaled energy, which in an experiment can be kept constant by changing energy and applied field simultaneously. The deformed sine waves appear clearly in a Fourier transform of a scaled energy spectrum with respect to $F^{-1/4}$. Such a Fourier transform (a recurrence spectrum) consists of a series of narrow resonances at the classical actions of the closed orbits of the system, with heights equal to their recurrence amplitudes.

Closed-orbit theory can be applied to nonhydrogenic atoms as well. Then a returning Coulomb wave (the returning electron) may not only be scattered back into the original orbit (Coulomb scattering), resulting in repeated traversals of this orbit, but also into other orbits as a result of core scattering [2]. When those core scattered waves are consistently accounted for in closed-orbit calculations, sum orbits appear as combinations of hydrogenic orbits. Furthermore, the intensity of the harmonics of hydrogenic recurrences will change (''core shadowing'') [5,6]. These core effects were observed in quantum calculations as well as in experiments on nonhydrogenic atoms [7–10].

The original formulation of closed-orbit theory in an electric field fails near bifurcations of the orbits parallel to the field direction. Above the zero-field ionization limit ($\epsilon = 0$), only the parallel orbit uphill the potential is closed. As the scaled energy is lowered from the zero-field ionization limit, new orbits are born in bifurcations from this orbit and its multiple traversals. At the bifurcation the uphill orbit (or one of its repetitions) and the newly created orbit are identical and have the same action. The semiclassical intensity diverges at this point. Recently Gao and Delos [1] derived a uniform approximation for the case of a hydrogen atom in an electric field in which these diverging intensities were corrected. Dando *et al.* [6] extended closed-orbit theory to nonhydrogenic atoms including core effects. They selected a scaled energy and $F^{-1/4}$ range where none of the orbits was close to its bifurcation. Shaw and Robicheaux [11] recently combined both theories, allowing calculations for nonhydrogenic atoms also near a bifurcation.

Bifurcation processes have to be studied in $M=0$ spectra. For $|M|>0$ the centrifugal barrier prohibits orbits along the field direction. Furthermore, in excitation from an s state, a node in the initially outgoing angular distribution determines that the strongest features in $|M|=1$ spectra result from orbits perpendicular to the field direction. These are observed far from their bifurcation.

Several groups reported results on scaled energy experiments on $M=0$ Rydberg atoms in an electric field. Eichmann *et al.* [12] performed scaled energy experiments at $\epsilon = -2.5$ on sodium in a two-step pulsed-laser excitation. From the $3p_{1/2}$ or $3p_{3/2}$ intermediate state they excited several m_l states simultaneously, depending on polarizations of the lasers of either $|m_l|=0$, 1, or 2 or $|m_l|=0$ or 1. The $m_l=0$ contribution was small; recurrence spectra were limited to low scaled actions due to their experimental energy resolution. Kuik *et al.* [13] recorded high-resolution scaled-energy spectra in barium. Rydberg series converging to the $5d_{3/2}$ and the $5d_{5/2}$ autoionization limits were investigated, in excitation from the $5d^2\,{}^1G_4$ metastable level. Several M states were excited simultaneously. Hydrogenic closed-orbit theory was used to interpret their data, but large deviations,

mainly in the intensities of the recurrence peaks, were observed. Courtney *et al.* [9,14] investigated bifurcation sequences over a wide range of scaled energies both above and below the saddle point in lithium. As a function of ϵ they studied the intensity dependences in the recurrence spectra around a bifurcation. They observed an increase from small, but nonzero before the bifurcation, via finite at the bifurcation, to a maximum intensity slightly after the bifurcation. Gao and Delos [1] used their refinement of closed-orbit theory to interpret the measured intensity dependence of the 1/2 and the 3/4 orbit close to their bifurcations from the second and fourth repetitions of the uphill orbit, respectively. Only the low action part of the spectrum was calculated and therefore effects of the lithium core could be neglected. Good agreement between theory and experiment was obtained.

In a previous paper [15] we presented results on $|M|=1$ scaled-energy spectra, investigating mainly effects of the helium core. In the present paper we will discuss results of scaled-energy spectroscopy on singlet helium $M=0$ Rydberg states. We recorded spectra at $\epsilon=-2.940(4)$ and $-2.350(4)$, both below the saddle point. Closed-orbit theory is applied for the interpretation of the data, including the correction for the diverging amplitudes described by Gao and Delos [1]; below the saddle point both the intensity of the uphill and downhill orbits may diverge as a result of nearby bifurcations. Furthermore, we investigated the high-action part of the spectrum, which will be influenced by the presence of the helium core. Core effects are expected to be much stronger in the $M=0$ case compared to our earlier $|M|=1$ spectra, due to the large ^1S quantum defect ($\delta_s=0.1397$), which is more than one order of magnitude larger than the singlet $l>0$ quantum defects. A description of core scattering, corrected for diverging amplitudes, requires an extension of closed-orbit theory. Recently this was accomplished by Shaw and Robicheaux [11]. Our helium $M=0$ spectra provide an excellent opportunity to compare their treatment with experimental spectra.

In Sec. II of this paper we briefly review scaled-energy spectroscopy and closed-orbit theory. In our previous paper [15] the ideas underlying the theory and basic equations, with emphasis on core effects, were discussed. Now we will concentrate more on the uniform approximation. In Sec. III the experimental setup will be described only briefly, since the same setup as in our previous paper on $|M|=1$ spectra is used. In Sec. IV measurements are presented. In Sec. V experimental recurrence spectra are compared with closed-orbit calculations. The paper ends with some conclusions in Sec. VI.

II. THEORY

A. Scaled Hamiltonian

The Hamiltonian for a hydrogen atom in an electric field with zero angular momentum along the field direction z is

$$H=\tfrac{1}{2}(p_z^2+p_\rho^2)-1/(\rho^2+z^2)^{1/2}+Fz. \tag{1}$$

When a scale transformation $\tilde{r}=rF^{1/2}$, $\tilde{p}=pF^{-1/4}$ is applied, a scaled Hamiltonian results:

$$\tilde{H}=H/\sqrt{F}=\tfrac{1}{2}(\tilde{p}_z^2+\tilde{p}_\rho^2)-1/(\tilde{\rho}^2+\tilde{z}^2)^{1/2}+\tilde{z}. \tag{2}$$

This scaled Hamiltonian no longer depends on energy and electric-field strength independently but solely on the scaled energy $\epsilon=E/\sqrt{F}$. The classical dynamics can be kept constant in an absorption experiment by changing energy and field simultaneously (scaled-energy experiment).

It is convenient to use a successive scale transformation to semiparabolic coordinates $u=\sqrt{\tilde{r}+\tilde{z}}$; $v=\sqrt{\tilde{r}-\tilde{z}}$ to circumvent the Coulomb singularity at the core when integrating the Hamilton equations. Closed orbits are searched by integrating the Hamilton equations of motion in these semiparabolic (u,v,p_u,p_v) coordinates. In steps of 0.001° the initial launching angle range between 0° and 180° is scanned.

B. Hydrogenic closed-orbit theory

The photoabsorption process and the subsequent electron motion is separated in two regimes of space: the region close to the core where a quantum description is required, and the region further out where a semiclassical description suffices. In the framework of closed-orbit theory an atom absorbs a photon and an electron leaves the core region as an outgoing Coulomb wave. Far from the core the electron can be viewed as a particle moving along a classical trajectory. Eventually this trajectory may curve back to the core, where again a quantum description is required. The electron then returns to the core region as an incoming Coulomb wave. If a trajectory returns exactly to the core a closed orbit is formed, and interference between the outgoing Coulomb wave and the returning wave in the direction of the returning orbit results in an oscillation in the absorption spectrum. The total absorption spectrum consists of a sum of deformed sine waves superimposed on a slowly varying background. The oscillatory part of the spectrum, composed of a sum of contributions of all closed orbits j, is given by

$$f(E)=\frac{-2(E-E_i)}{\pi}\mathrm{Im}\sum_j N_j\sqrt{8}\pi Y(\theta). \tag{3}$$

Here $(E-E_i)$ is the energy with respect to the zero-field ionization limit E_i, $Y(\theta)$ is the angular distribution of the outgoing Coulomb wave, and θ is the launching angle of the orbit with respect to the positive z axis. $Y(\theta)\propto\cos\theta$ when $M=0$ final states are excited from an S state [see Eq. (2.6) Ref. [4]]. N_j is calculated by matching the semiclassical and quantum expressions at the core radius. For the uphill and downhill orbits N_j is given by

$$N_j=-4\pi Y(\theta)\frac{F^{1/4}}{\sqrt{2}J_{12}}\times e^{i(2\pi\tilde{S}_jF^{-1/4}-\mu_j\pi/2-\pi/2)}. \tag{4}$$

For all other orbits N_j is given by

$$N_j=-2^{9/4}\pi^{3/2}Y(\theta)\frac{\sin\theta}{\cos(\theta/2)}\frac{F^{1/8}}{(\sqrt{2}J_{12})^{1/2}}\times e^{i(2\pi\tilde{S}_jF^{-1/4}-\mu_j\pi/2-3\pi/4)}. \tag{5}$$

In Eqs. (4) and (5), S_j and μ_j are, respectively, the classical scaled action and the Maslov index of the orbit. J_{12} determines the stability of the orbit. For the uphill and downhill orbits,

$$J_{12}=\frac{|\sin(\sqrt{2\epsilon}n\tau)|}{\sqrt{2\epsilon}}. \tag{6}$$

Here τ is the recurrence time of the first traversal of the uphill (downhill) orbit. J_{12} is zero when $\sqrt{2\epsilon}n\tau$ is a multiple of π. The intensity of the nth repetition of the uphill (downhill) orbit diverges when n is a multiple of $n_0=\pi/(\sqrt{2\epsilon}\tau)$. At this scaled energy a bifurcation from the nth repetition of the uphill or downhill orbit occurs. The larger the $1/J_{12}$ for a repeated traversal of the uphill or downhill orbit, the closer this orbit is to a bifurcation. Then unphysical diverging amplitudes contribute to the summation over closed orbits, and consequently the original formulation of closed-orbit theory fails in the neighborhood of bifurcations.

Each orbit emerges from a bifurcation of the uphill orbit (straight-line orbit along the u axis) when ϵ is lowered from the zero-field ionization limit at $\epsilon=0$. New orbits are labeled by a rational number m/n which characterizes their shape. An m/n orbit returns m times to $u=0$ (m periods of v motion) and n times to $v=0$ (n periods of u motion) before it closes. It emerges as a bifurcation from the nth repetition of the uphill orbit. At its bifurcation the newly created orbit and the uphill orbit coincide. When ϵ is lowered further, the initial momentum in the v direction p_v grows from zero at the bifurcation to

$$p_v=2\sin(\theta/2), \tag{7}$$

where θ is the launching angle of the new orbit. Finally at some value of ϵ below the saddle point ($\epsilon=-2$) this orbit coincides with the downhill orbit (straight-line orbit along the v direction) and disappears in an inverse bifurcation. An m/n orbit is destroyed by the mth repetition of the downhill orbit. The uphill (downhill) and adjacent orbits form a cusplike structure upon return to the core. At the bifurcation the tip of this cusp touches the core. From this moment onwards one of the adjacent orbits becomes closed as well: the newly created orbit. This focusing effect, which causes the divergence in the semiclassical amplitude, is found in other fields of physics as well. For instance, in geometrical optics, when a plane wave is focused to a point, the intensity diverges in the focus point. A correct description would account for a finite size of the focus resulting from diffraction. For this purpose, integrals of the Fresnel type are usually used to correct geometrical optics. Gao and Delos [1] introduced a similar solution (the uniform approximation) for a system of an atom in an electric field. They applied this approximation to orbits close to their bifurcation from the uphill orbit or one of its repetitions. Replacing v and p_v by u and p_u, their expressions can be applied close to inverse bifurcations from the downhill orbit as well [16]. The derivation is long; however, the final expressions required in the calculation are simple and will be reproduced below.

The oscillator strength density in the uniform approximation, representing both the effects of the uphill or downhill orbit (or one of their repetitions) and a new orbit close to a bifurcation, is given by

$$f(E)=(E-E_i)\pi 2^3\times\mathrm{Im}[I(\lambda,a)e^{i(2\pi\tilde{S}_0F^{-1/4}-\mu_0\pi/2-\pi)}]. \tag{8}$$

Here S_0 is the classical action of the uphill or downhill orbit (or one of their repetitions), and μ_0 its Maslov index before the bifurcation. Furthermore the integral $I(\lambda,a)$ is given by

$$\begin{aligned} I(\lambda,a)=&\sqrt{\frac{\pi}{\lambda}}e^{-i(a_1^2/4a_3)F^{-1/4}}g(-a)\\ &\times\left[\frac{1}{2}-C\left(\sqrt{\frac{\lambda}{\pi}}a\right)+\frac{1}{2}i-S\left(\sqrt{\frac{\lambda}{\pi}}a\right)i\right]\\ &+\frac{i}{\lambda}g'(-a). \end{aligned} \tag{9}$$

The first term on the right-hand side of Eq. (9) contains the Fresnel integrals $C(s)=\int_0^s\cos(\pi t^2/2)dt$ and $S(s)=\int_0^s\sin(\pi t^2/2)dt$. The second term is the Bleistein correction term, which is much smaller than the first term. a relates to p_v of the new orbit upon a return to the core: $p_v=\sqrt{-a}$. Furthermore, $a=a_1/a_3$. a_1 is a parameter depending on the distance from the bifurcation:

$$a_1=\frac{\sin(\sqrt{2\epsilon}n\tau)}{\sqrt{2\epsilon}\cos(\sqrt{2\epsilon}n\tau)}. \tag{10}$$

a_3 can be deduced from the new orbit and a_1 using Eq. (7). $\lambda=-0.5a_3F^{-1/4}$, and $g(-a)$ is the value of $g(p_v^2)$ at the new orbit. The derivative of $g(p_v^2)$ at the new orbit, $g'(-a)$, is approximated by

$$g'(-a)=\frac{g(-a)-g(0)}{-a}. \tag{11}$$

$g(-a)$ and $g(0)$ [which relate to (the repeated traversal of) the uphill orbit] are given by

$$g(0)=Y(0)Y(0)\left|\frac{a_1}{J_{12,0}}\right|, \tag{12}$$

$$g(-a)=Y(\theta)Y(\theta)\left|\frac{2a_1}{J_{12,\mathrm{new}}}\right|^{1/2}. \tag{13}$$

Before the bifurcation, a_3 and $g(-a)$, which relate to the new orbit, are extrapolated from their values after the bifurcation, when the orbit is real. In Eq. (9), $a_1^2/4a_3$ corresponds to the action difference between the uphill (or downhill) orbit (or one of its repetitions) and the new orbit. Close to the bifurcation, where the uphill and new orbit contributions are not yet resolved, the corresponding exponentional term results in a shift of the peak position toward lower action compared with the uphill (downhill) orbit action. Far from the bifurcation the conventional closed-orbit result and the uniform approximation coincide.

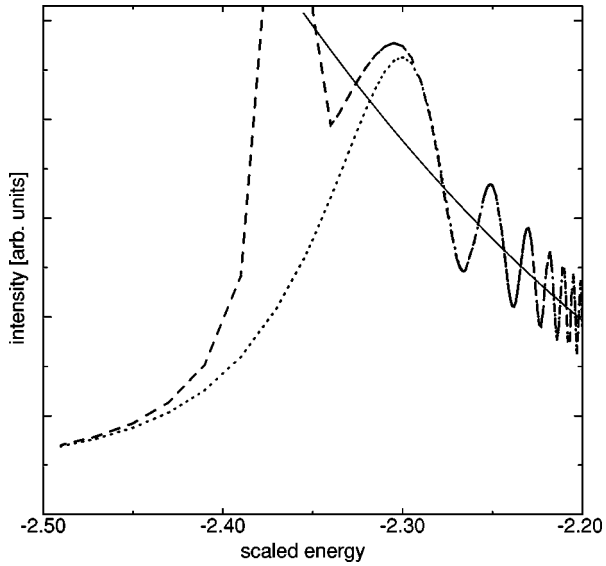

FIG. 1. The intensity of the fourth repetition of the downhill orbit close to the bifurcation of the $\frac{4}{5}$ orbit, $(130.15<F^{-1/4}<155.90)$. Dashed line, conventional closed-orbit calculation; dotted line, uniform approximation; full line, contribution of the new orbit.

In Fig. 1 the intensity dependence of the fourth repetition of the downhill orbit ($\theta=180°$) is shown for ϵ between -2.5 and -2.2, around the bifurcation of the $\frac{4}{5}$ orbit. The dashed line represents the conventional closed-orbit result. The dotted line results when the uniform approximation is used. The 4/5 orbit bifurcates at $\epsilon=-2.359$, which is close to $\epsilon=-2.350$, where one of our spectra is recorded. Approaching the bifurcation from the left (low ϵ) the conventional closed-orbit result grows, and diverges at the bifurcation. After the bifurcation the intensity decreases while oscillating. The intensity decreases mainly because the initial angle of the new orbit grows, and $Y(\theta)$ decreases with θ in $M=0$ spectra. This effect is shown by the full line in Fig. 1, where the contribution of the new orbit to the intensity is plotted. The oscillations result from interference with the downhill orbit, and become smaller as the contribution of the downhill orbit decreases away from the bifurcation. Finally the intensity vanishes. At low ϵ the conventional result and uniform approximation are identical. On approaching the bifurcation the uniform approximation starts to deviate from the conventional result. At the bifurcation the corrected intensity is finite. The intensity is largest after the bifurcation (at $\epsilon=-2.30$), and then drops while oscillating. From $\epsilon=-2.29$ on, conventional closed-orbit theory and the uniform approximation coincide again. At this scaled energy the initial angle of the new orbit is approximately as large as 146°, and the new orbit already deviates geometrically significantly from the fourth repetition of the downhill orbit.

C. Closed-orbit theory for helium

In Sec. II B, a closed-orbit theory for hydrogen was described. When core scattered waves are taken into account, closed-orbit theory can be used to describe the recurrence spectra of nonhydrogenic atoms as well [5,6]. However, the procedure of Dando *et al.* [5,6], that was used in our previous paper on $|M|=1$ spectra [15], is not directly applicable. The expressions in Refs. [5] and [6] cannot be applied to combinations of orbits that need correction for diverging amplitudes. For $M=0$ spectra many such corrections are necessary. Shaw and Robicheaux [11] recently published expressions that incorporate these core scattering effects close to bifurcations. They make a partial wave expansion of the core scattered wave in the neighborhood of a bifurcation, and use it in a derivation similar to the uniform approximation of Gao and Delos [1], to arrive at a description for nonhydrogenic atoms close to bifurcations.

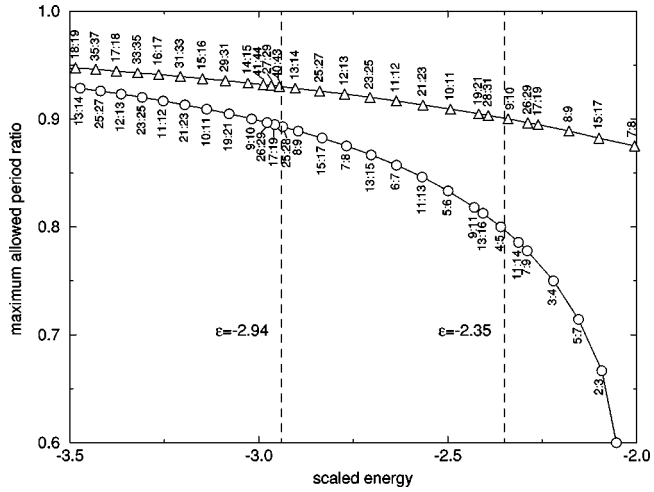

FIG. 2. The maximum allowed period ratio for uphill and downhill orbits, respectively. $n/(n+1)$ and $n/(n+2)$ bifurcation energies are shown. Around $\epsilon=-2.94$ and $\epsilon=-2.35$, several $n/(n+3)$ bifurcation energies are also shown.

D. Numerical calculations

A constant-scaled-energy spectrum is constructed by summing the oscillations given by Eq. (3), with their intensities, classical actions, and additional phases. The spectrum is then Fourier transformed with respect to $F^{-1/4}$, and compared with a Fourier transform of the experimental spectrum up to the highest scaled action for which orbits were searched. An orbit is created in a bifurcation as soon as its period ratio m/n equals the maximum allowed period ratio, which depends on ϵ. In Fig. 2 the maximum allowed period ratio is shown as a function of ϵ for both the uphill (upper curve) and the downhill (lower curve) orbits from $\epsilon=-3.5$ to -2.0. The bifurcations of the $n/(n+1)$ and $n/(n+2)$ orbits are indicated in the figure (triangles and circles for bifurcations from the uphill and downhill orbits, respectively). Around $\epsilon=-2.94$ and -2.35, bifurcations of $n/(n+3)$ orbits are shown as well. Orbits resulting in peaks in the high-action part of the spectrum have period ratios with large denominators. Therefore, the period ratios of successive bifurcating orbits differ only slightly here. Successive bifurcations occur rapidly, and can no longer be considered isolated [9]. This leads to problems in the calculations. Shaw and Robicheaux [16] mentioned similar calculational problems around $\epsilon=-2$ even in the low-action part of the spectrum. In our spectra we expect the first problems for bifurcations of repeated traversals of the downhill orbit at $\epsilon=-2.35$, as the

curve of the maximum allowed period ratio as a function of ϵ is steepest here. Shaw and Robicheaux argued that the uniform approximation is required, when the difference in actions of a new orbit ($S_{\rm new}$) and a downhill orbit (S_{D_n}), fulfills the inequality

$$2\pi|\tilde{S}_{\rm new}-\tilde{S}_{D_n}|\leqslant F^{1/4}. \tag{14}$$

Calculational results presented in this paper are limited to $\tilde{S}<20$. Applying inequality (14) to the D_{39} orbit at $\tilde{S}=19.78$ ($\epsilon=-2.35$), we find that the uniform approximation is only required for one of the orbits that bifurcates out of it near $\epsilon=-2.35$. From this observation we conclude that successive bifurcations can be assumed to be isolated for all orbits with $\tilde{S}<20$ considered in this paper.

III. EXPERIMENT

Our experimental setup was described in detail in a previous paper on scaled-energy spectroscopy of helium $|M|=1$ states [15]. Here we will only give a brief summary. A beam of metastable helium atoms is produced by running a dc discharge through an expanding gas flow. The beam is collimated by a skimmer and a horizontal and vertical slit pair. Downstream the beam is perpendicularly intersected by the UV output (8 mW, 312 nm) of an intracavity frequency-doubled cw rhodamine B ring dye laser, pumped by an Ar^+ laser. The metastables are excited from the $1s2s\ ^1S_0$ state to $1snp\ ^1P_1$ Rydberg states ($F=0$). The polarization direction of the laser was parallel to the field direction to excite $M=0$ final states. The interaction region is localized in a stainless-steel box in which an electric field along the beam direction is applied. Rydberg atoms that survive this interaction region are field ionized downstream underneath a channeltron electron multiplier, and detected. The direction of the field in the interaction region is chosen such that electrons, detached from Rydberg atoms that do not survive the interaction region, are expelled toward the electron multiplier, and counted as well.

To keep ϵ constant during a laser scan, the excitation energy has to be known accurately. A zero-field transition, recorded before the electric field is switched on, serves as an absolute energy marker. Simultaneously recorded transmission peaks of the red output of the ring dye laser through an actively length-stabilized 150-MHz confocal etalon are used for calibration with respect to the zero-field absorption peak. The applied field is online controlled by a Sun sparc workstation. The output of a digital-to-analog convertor is applied over two capacitor plates in the interaction region. The estimated absolute accuracy in ϵ is 0.004, mainly determined by the uncertainty in the field calibration. ϵ is estimated to be constant within 0.001. Spectra are recorded between the $n=50$ and 80 zero-field transitions. Since the scan range of the laser is limited to 40 GHz, about ten overlapping scans are recorded. The spectra are linked and Fourier transformed with respect to $F^{-1/4}$. The long energy range is needed to achieve good resolution in the recurrence spectra. The average value of $F^{-1/4}$ is approximately 145.

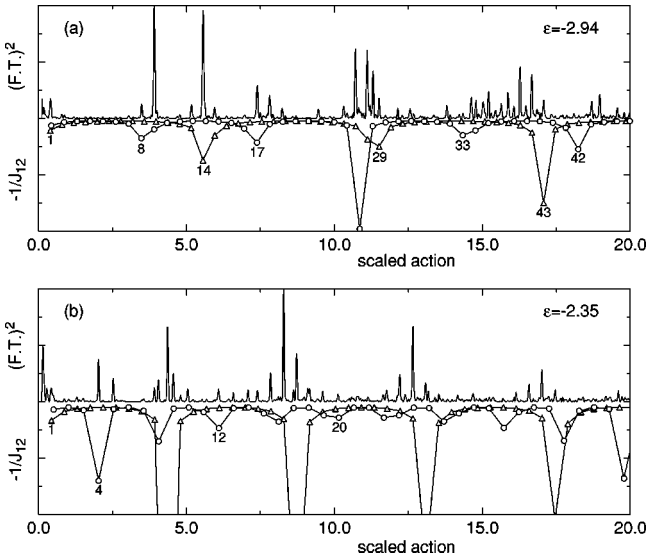

FIG. 3. Square of the Fourier transform of experimental spectra [(F.T.)^2] compared to calculated values of $1/J_{12}$ for repetitions of the uphill (triangles) and downhill (circles) orbits (all in arb. units) (a) at $\epsilon=-2.94$ and (b) at $\epsilon=-2.35$.

IV. MEASUREMENTS

We performed scaled-energy experiments at $\epsilon=-2.940(4)$ ($135.86<F^{-1/4}<160.11$) and at $\epsilon=-2.350(4)$($130.15<F^{-1/4}<155.90$). Fourier transforms of the experimental spectra are shown in the upper part of Figs. 3(a) and 3(b) for $\epsilon=-2.94$ and -2.35, respectively. The Fourier transforms, as a function of the scaled action, consist of narrow resonances with a full width at half maximum of 0.05. In the low-action part of the Fourier transforms one short action resonance is clearly visible. It corresponds to the unresolved first traversal of the uphill and downhill orbits (for $\epsilon=-2.94$, $\tilde{S}_{U_1}=0.3970$ and $\tilde{S}_{D_1}=0.4343$; and for $\epsilon=-2.35$, $\tilde{S}_{U_1}=0.4363$ and $\tilde{S}_{D_1}=0.5073$). At low action some noise is also present which results from the slightly varying backgrounds in the overlapping laser scans. At higher actions most peaks appear at positions that are multiples of the uphill (U_n) or downhill (D_n) orbit. Other orbits contribute as well. However, in $M=0$ spectra, they have the largest intensity close to their bifurcation, where it is difficult to distinguish them from repetitions of the uphill or downhill orbit.

In Fig. 3 the experimental recurrence spectra are compared with calculated values of $1/J_{12}$ for the repeated traversals of the uphill (triangles) and downhill (circles) orbits. From Eq. (4) it follows that $1/J_{12}$ determines the relative recurrence strength of the repeated traversals in the original formulation of closed-orbit theory. The values of $1/J_{12}$ show at a glance which orbits are close to a bifurcation, as at their scaled action $1/J_{12}$ is large. Precisely at a bifurcation, $1/J_{12}$ diverges. Here n is a multiple of n_0, which is 1.075 and 0.893 at $\epsilon=-2.94$ and 1.111 and 0.796 at $\epsilon=-2.35$ for uphill and downhill orbits, respectively. In general the most intense peaks in the experimental recurrence spectra occur at the high-action side of the maxima in $1/J_{12}$ for repetitions of the downhill orbit and at the low-action side of the maxima in $1/J_{12}$ for repetitions of the uphill orbit. Here new orbits

just bifurcate, and the intensity reaches a maximum (see Fig. 1). For instance, at $\epsilon=-2.94$ the intensity of the experimental peak at the action of the ninth repetition of the downhill orbit ($\widetilde{S_{U_9}}=-3.906$) is large. Indeed, Fig. 2 shows that the 9/10 orbit exists but will soon be destroyed by the ninth repetition of the downhill orbit when lowering ϵ. The intensity of other peaks in our spectra at actions of the uphill (or downhill) orbits and their repetitions can be understood in a similar way. The separation between successive maxima in $1/J_{12}$ is smaller for the downhill orbit than for the uphill orbit. This can be understood from Fig. 2 as well. The curve representing the maximum allowed period ratio as a function of ϵ is steeper for the downhill orbit. Therefore, bifurcations are more frequent in this case. From similar arguments it is understood that successive maxima for $\epsilon=-2.35$ lie closer together than for $\epsilon=-2.94$, both for repetitions from the uphill and downhill orbits.

Spectra far above the saddle point could not be recorded. The signal strength dropped rapidly above the saddle point, and no $M=0$ spectra with reasonable signal strength could be recorded for $\epsilon>-1.990$. When crossing the saddle point the peaks in the frequency spectrum broaden, and rapidly disappear in the smoothly varying continuum. It was, however, possible to record $|M|=1$ spectra far above the saddle point (which, for $|M|=1$, is slightly shifted from $\epsilon=-2$), although the signal strength at $\epsilon=-1.76$ was weaker than at $\epsilon=-2.35$ and -2.94 [15]. Peaks in the $|M|=1$ spectra therefore correspond to states that live longer than in $M=0$ spectra. The most dominant contribution to $|M|=1$ spectra arises from orbits leaving the core perpendicularly to the field direction, while the strongest excitation for $M=0$ is in the field direction (uphill or downhill). Electrons leaving the core toward the saddle point can escape directly. Nevertheless the almost steplike drop in signal strength directly above the saddle point is surprising. We are convinced that it is not the detection method that induces the drop in signal strength. The detection region is situated directly behind the excitation region in our experimental setup. The applied field direction was chosen such that electrons, detached from atoms that are ionized in the interaction region, are expelled into the detection region and detected.

V. COMPARISON WITH CLOSED-ORBIT THEORY

In Fig. 4(a) a conventional closed-orbit calculation for hydrogen at $\epsilon=-2.94$ is shown. When comparing this calculation with the Fourier transform of the experimental spectrum [Fig. 4(d)], we can clearly see the problematic actions where the semiclassical intensity diverges (for instance for U_{14} and D_{25}).

In Fig. 4(b) a closed-orbit calculation, where 15 diverging amplitudes are corrected, using the uniform approximation, is shown. Many such corrections were required; the corrected peaks are marked with a dot in the figure. The calculations clearly show much better agreement with the experimental spectrum at least up to $\tilde{S}=12.0$. Also, in the higher-action part, the use of the improved hydrogen theory results in a better agreement in intensity for most of the peaks. A quite dramatic improvement is achieved, for instance, for the intensity of the 25th repetition of the downhill orbit (D_{25}).

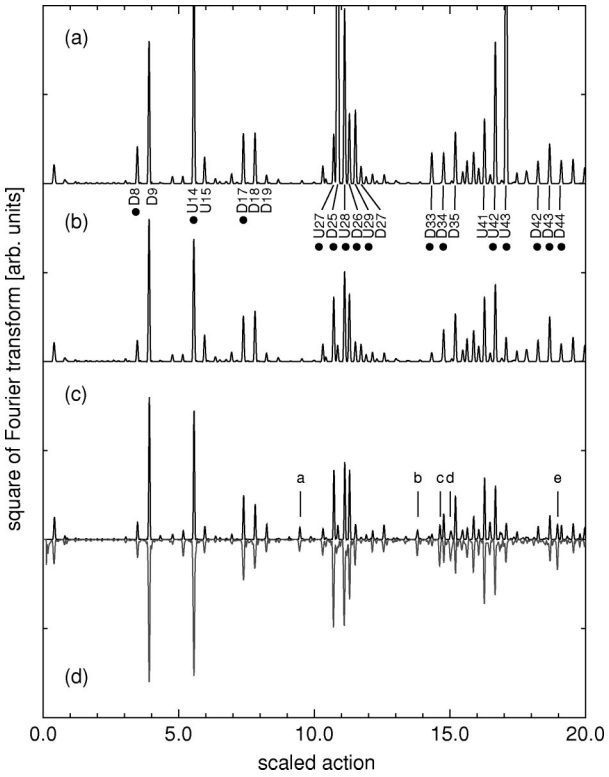

FIG. 4. Recurrence spectra at $\epsilon=-2.94$. (a) Conventional closed-orbit calculation for hydrogen. (b) Closed-orbit calculation with diverging amplitudes corrected (marked with a dot) for hydrogen (uniform approximation). (c) Closed-orbit calculation for helium. (d) Fourier transform of an experimental scaled energy spectrum for singlet helium.

This, in standard closed-orbit theory, highly overestimated peak becomes small when using the uniform approximation. In Fig. 2 we see that the bifurcation of the 25/28 orbit, which does not yet exist at $\epsilon=-2.94$, is very near. Just before the bifurcation the conventional result overestimates the intensity strongly while the corrected result is still relatively small (compare with Fig. 1).

We find extra peaks in our experimental spectrum that cannot be explained with hydrogenic closed-orbit theory. In Fig. 4(c) a closed-orbit calculation for helium is shown. The ''extra peaks'' reproduced in this calculation, labeled *a*–*e* in Fig. 4(c), can be attributed to sum orbits induced by scattering on the He^+ core. When only combinations of two orbits are considered, peak *a* corresponds to $D_9 \oplus U_{14}$, peak *b* to $D_{19} \oplus U_{14}$ and/or $D_{18} \oplus U_{15}$, peak *c* to $D_8 \oplus U_{28}$, peak *d* to $D_9 \oplus U_{28}$, and peak *e* to $D_{18} \oplus U_{28}$. They are all combinations of the strongest hydrogenic peaks in the spectrum. A second core effect (''core shadowing'') causes a change in the intensity of hydrogenic orbits. As the intensity of most peaks in the calculation for hydrogen already agreed quite well with the experimental results, the impact of this effect must be small. However for, e.g., D_{18}, which contributes to core scattering, the agreement with experiment improves significantly by including core effects. The clearest example of core shadowing is the almost complete disappearance of the 27th repetition of the downhill orbit (D_{27}), when the core is taken into account in the calculation. The agreement between the experimental recurrence spectrum and the closed-orbit calculation for helium is now very good. In our previous

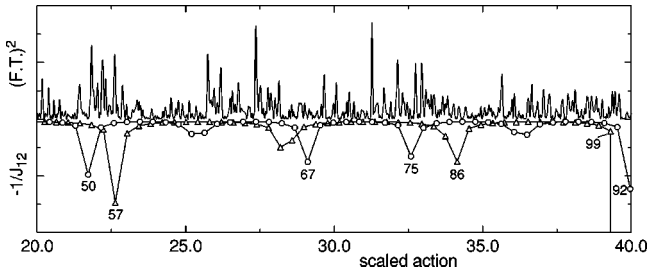

FIG. 5. High action part of the square of the Fourier transform of the experimental spectrum $[(\mathrm{F.T.})^2]$ at $\epsilon=-2.940(4)$ compared to calculated values of $1/J_{12}$ for repetitions of the uphill (triangles) and downhill (circles) orbits (all in arb. units).

paper on $|M|=1$ spectra and in a recent paper by Keeler and Morgan [17], only intensity changes as a result of the core were observed. Since an $|M|=1$ hydrogenic spectrum contains groups of equidistant peaks, all sum orbits coincide with hydrogenic orbits already present in the spectrum. In an $M=0$ spectrum a peak is either at the position of a repetition of the uphill or downhill orbit. A combination orbit consisting of a repetition of the uphill orbit and one of the downhill orbit results in an extra peak in this case.

The positions of observed peaks are expected to be close to but not exactly at the actions corresponding to (repetitions of) the uphill and downhill orbits. Emerging orbits shift these peak positions toward lower actions. The further away from the bifurcation, the larger such a shift is. However, far from a bifurcation the intensity of most peaks is too small to determine their positions accurately. The observation of such a shift relies on the observation of not too small a peak far from its bifurcation. However, no such peak contributes to the spectrum at $\epsilon=-2.94$. Deviations between experimental and calculated peak positions of 0.004 and 0.008 can be explained, considering the accuracy in ϵ, for $n/(n+1)$ and $n/(n+2)$ orbits [including first repetitions of $n/(n+1)$ orbits], respectively. Since the full width at half maximum of the peaks is 0.05, the peak positions of the strongest peaks can be determined with an accuracy of 0.005. Experimental peak positions agreed with calculated values within this experimental accuracy in all cases.

In Fig. 5 the high-action part of the experimental recurrence spectrum at $\epsilon=-2.940(4)$ is shown. The experimental recurrence strength is multiplied by a factor 3 with respect to the strength in Fig. 3. $1/J_{12}$ is shown for the repetitions of the uphill and downhill orbits for this part of the spectrum as well. Most of the intense peaks are found on the high- and low-action sides of the maxima in $1/J_{12}$ for repetitions of the downhill and uphill orbits, respectively (as in the low-action part of the spectrum). Core scattering may result in peaks outside those ranges. Interpretation of the higher-action part of the spectrum is more difficult, as it is more sensitive to the precise value of the scaled energy. Deviations of 0.03 in action can be understood here within the accuracy of ϵ for $\tilde{S}>30$. Many peaks have a position which corresponds, within the experimental accuracy, to the action of a repeated traversal of the uphill or downhill orbit. As bifurcations appear more rapidly for higher actions, more orbits contribute and interfere, resulting in a larger influence on the intensities as well. Orbits with actions corresponding to the 200th repetition of the uphill and downhill orbits could easily be observed.

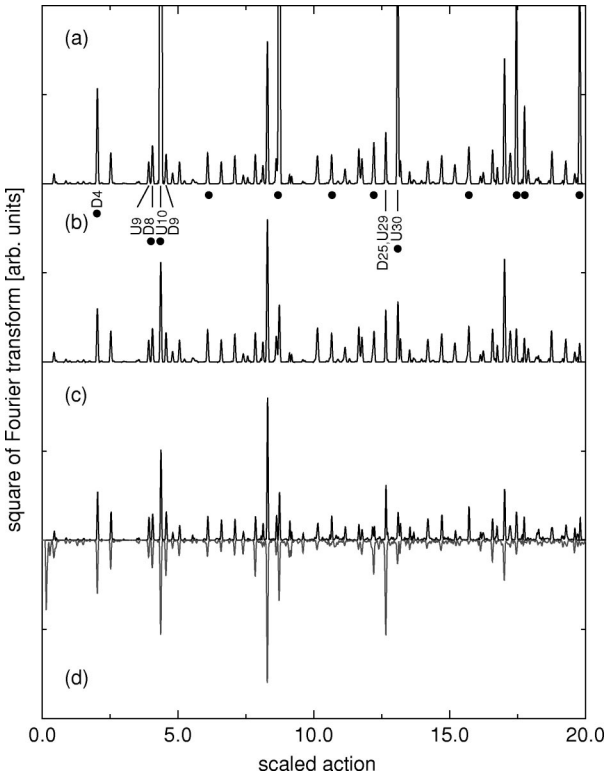

FIG. 6. Recurrence spectra at $\epsilon=-2.35$. (a) Conventional closed-orbit calculation for hydrogen. (b) Closed-orbit calculation with diverging amplitudes corrected (marked with a dot) for hydrogen (uniform approximation). (c) Closed-orbit calculation for helium. (d) Fourier transform of an experimental scaled energy spectrum for singlet helium.

In Fig. 6(a) a conventional closed-orbit calculation for hydrogen at $\epsilon=-2.347$ is shown. Again the positions of the calculated orbits match perfectly with the measured values. Many peaks need corrections for diverging amplitudes at this scaled energy as well. We chose $\epsilon=-2.347$ instead of $\epsilon=-2.350$ because (within the error margins of 0.004) for this value best agreement was found between our $|M|=1$ spectra and calculations [15]. In Fig. 6(b) a closed-orbit calculation for hydrogen in the uniform approximation is shown. Corrected peaks are marked with a dot. The agreement between calculation and experiment significantly improved for this scaled energy as well. Up to $\tilde{S}=10$ a perfect agreement between closed-orbit calculation and experiment is achieved. The agreement for high actions is also quite good, although small differences remain. For instance, the peak intensity at $\tilde{S}=12.6$, which turned out to be extremely sensitive for the value of ϵ, is underestimated. D_{25} and its bifurcated 25/31 orbit (at $\epsilon=-2.383$) and U_{29} and its bifurcated 26/29 orbit (at $\epsilon=-2.288$) contribute to this peak. The resulting interference leads to a large sensitivity for ϵ here. A minimum in the calculated intensity occurs for $\epsilon=-2.347$ and -2.351. This observation allows us to deduce that the scaled energy differs slightly from $\epsilon=-2.347$, and probably has a value somewhere in between $\epsilon=-2.347$ and -2.351.

In the spectrum recorded at $\epsilon=-2.35$ no extra peaks

were found that could be attributed to sum orbits. A closed-orbit recurrence spectrum for helium confirming the absence of intense sum orbits, is shown in Fig. 6(c). Effects of core shadowing are observed again, e.g., in the decrease in the intensity of the 30th repetition of the uphill orbit (U_{30}). In the previous paper on $|M|=1$ spectra we also observed a decrease in the influence of the core on the spectra when ϵ was increased. The importance of core effects depends on the value of the quantum defect and on the $F^{-1/4}$ range over which the spectrum is recorded. In general, core effects will be more pronounced for smaller $F^{-1/4}$. The $F^{-1/4}$ ranges studied in the present experiment, however, do not differ enough to explain the observed diminishing effect of core scattering with increased value of ϵ.

VI. CONCLUSIONS

We presented measurements of constant-scaled-energy spectra of helium atoms in an electric field. Closed-orbit theory is used for a interpretation of these spectra. The $M=0$ spectra require the application of the uniform approximation to repair divergences occurring in the original formulation of closed-orbit theory. Small extra peaks in the recurrence spectra are attributed to core scattering. The most recent extension of closed-orbit theory [11] now explains the spectra up to $\tilde{S}=20$ for $\epsilon=-2.94$ and up to $\tilde{S}=12$ for $\epsilon=-2.35$. Theoretical improvement of closed-orbit theory is required in cases where successive bifurcations have to be considered simultaneously. This will occur always for sufficiently high action. On the other hand, at increased action the experimental accuracy is lower as ϵ variations over the spectrum become more and more important. This induces intensity variations of, especially, interfering orbits.

Closed-orbit theory for helium requires only the incorporation of one or two small quantum defects. The present work shows that the inclusion of these quantum defects into the theory works very well. It remains to be seen, however, how well closed-orbit theory describes heavier elements with a larger core. This will be a subject of further study in our laboratory.

ACKNOWLEDGMENTS

We thank J. Bouma for his essential technical support. Furthermore, we gratefully acknowledge J. Shaw for his quick response to questions concerning the implementation of the uniform approximation in our computer code and for performing the closed-orbit calculations for helium presented in this paper.

[1] J. Gao and J. B. Delos, Phys. Rev. A **56**, 356 (1997).
[2] J. Gao and J. B. Delos, Phys. Rev. A **49**, 869 (1994).
[3] J. Gao, J. B. Delos, and M. Baruch, Phys. Rev. A **46**, 1449 (1992).
[4] J. Gao and J. B. Delos, Phys. Rev. A **46**, 1455 (1992).
[5] P. A. Dando, T. S. Monteiro, D. Delande, and K. T. Taylor, Phys. Rev. Lett. **74**, 1099 (1995).
[6] P. A. Dando, T. S. Monteiro, D. Delande, and K. T. Taylor, Phys. Rev. A **54**, 127 (1996).
[7] D. Delande, K. T. Taylor, M. H. Halley, T. van der Veldt, W. Vassen, and W. Hogervorst, J. Phys. B **27**, 2771 (1994).
[8] G. Raithel, H. Held, L. Marmet, and H. Walther, J. Phys. B **27**, 2849 (1994).
[9] M. Courtney, N. Spellmeyer, H. Jiao, and D. Kleppner, Phys. Rev. A **51**, 3604 (1995).
[10] T. S. Monteiro and G. Wunner, Phys. Rev. Lett. **65**, 1100 (1990).
[11] J. Shaw and F. Robicheaux, Phys. Rev. A **58**, 3561 (1998).
[12] U. Eichmann, K. Richter, D. Wintgen, and W. Sandner, Phys. Rev. Lett. **61**, 2438 (1988).
[13] G. J. Kuik, A. Kips, W. Vassen, and W. Hogervorst, J. Phys. B **29**, 2159 (1996).
[14] M. Courtney, J. Hong, N. Spellmeyer, D. Kleppner, J. Gao, and J. B. Delos, Phys. Rev. Lett. **74**, 1538 (1995).
[15] A. Kips, W. Vassen, W. Hogervorst, and P. A. Dando, Phys. Rev. A **58**, 3043 (1998).
[16] J. A. Shaw and F. Robicheaux, Phys. Rev. A **58**, 1910 (1998).
[17] M. Keeler and T. J. Morgan, Phys. Rev. Lett. **80**, 5726 (1998).